Influence of Bi addition on the optical properties of $As_{40}Se_{60}$ thin films

Mukta Behera*, Rozalin Panda, Naresh C. Mishra, Ramakanta Naik

Department of Physics, Utkal University, Bhubaneswar, 751004, India

*Corresponding author, E-mail: muktaphysics@gmail.com; Tel: (+91) 9439455986

Received: 31 March 2016, Revised: 02 August 2016 and Accepted: 08 September 2016

DOI: 10.5185/amp.2016/216
www.vbripress.com/amp

Abstract

In the present work, structural, microstructural, compositional and electronic band gap properties of $As_{40}Se_{60}$ and $As_{40}Bi_{15}Se_{45}$ bulk and thin films are reported. The films were prepared by thermal evaporation technique under high vacuum. X-ray diffraction (XRD) study indicated amorphous nature of $As_{40}Se_{60}$ in bulk prepared by melt quenching technique. Bi incorporation in $As_{40}Se_{60}$ with composition $Bi_{15}As_{40}Se_{45}$ however led to nucleation of Bi_2Se_3 nanocrystallites in the amorphous matrix of $As_{40}Se_{60}$. The films made out of the two targets of composition $As_{40}Se_{60}$ and $As_{40}Bi_{15}Se_{45}$ did not show any XRD peak, indicating their amorphous nature. UV-Visible-NIR spectroscopic study indicated a large decrease in the electronic band gap from 1.74 eV in films of composition $As_{40}Se_{60}$ to 1.28 eV for compositon $Bi_{15}As_{40}Se_{45}$. This decrease is explained on the basis of a high concentration of defect states leading to the presence of localized states in the band gap due to Bi incorporation. Field emission scanning electron microscopy (FESEM) images show smooth and homogeneous surface for the $As_{40}Se_{60}$ films, while Bi incorporation led to increases of the surface roughness in the $Bi_{15}As_{40}Se_{45}$ films. The decreased band gap and increased surface roughness on Bi incorporation in $As_{40}Se_{60}$ films indicate the suitability of these films for solar cell applications.

Keywords: Amorphous semiconductor, chalcogenide, thin film, nanocrystallites, band gap.

Introduction

Chalcogenide semiconducting glasses are important class of amorphous semiconductors. They have found applications as IR transmitting materials [**1–3**], filters, anti-reflection coatings and a wide range of optical devices [**4-6**] due to their novel electrical, thermal and optical properties. $As_{40}Se_{60}$ occupies a special place among all the binary chalcogenide families because of its widest glass forming region [**7**]. This material has been extensively used in optical fiber, optical gratings, micro lenses, holographic media, optical memories, nonlinear optical elements etc. [**8-10**]. The glassy chalcogenide semiconductor's properties are affected by the addition of a third element [**11, 12**]. Metallic impurities such as Pb and Bi in particular produce a remarkable change in the electrical and optical properties of $As_{40}Se_{60}$ glasses. The different electronegativity of Bi as compared to that of the host As-Se matrix is expected to affect the structure of the host and hence its electrical and optical properties [**13**]. Generally, chalcogenides are p-type semiconductors. Bi incorporation transforms this p-type material to n type **[14-16].** However, the role of Bi in transforming the electrical conduction from p to n type has still remained elusive [**15**]. In the present work Bi has been chosen as an additive element in As-Se alloys. Considering the importance of Bi_2Se_3 as a thermo-electric material [**17**] and topological insulator [**18**], we probed into the effect of Bi addition on the different characteristics of As-Se in bulk and thin film forms. While $As_{40}Se_{60}$ bulk melt quenched samples exhibit glassy behavior, Bi incorporation with composition of $As_{40}Bi_{15}Se_{45}$ leads to nucleation of Bi_2Se_3 nanocrystals embedded in the glassy matrix. Thin films of both the compounds exhibit glassy behavior. Incorporation of Bi is shown to have a profound effect on the optical band gap of $As_{40}Se_{60}$. The optical absorption coefficient in particular increases on Bi doping, thus indicating the suitability of this material for optical memory devices as well as in solar cells [**19**].

Experimental

Materials

The materials of the present study are $As_{40}Se_{60}$ and $Bi_{15}As_{40}Se_{45}$ in both bulk and thin film forms. The precursors used for the preparation of these materials were As, Se and Bi powder of high purity (99.999%, Sigma-Aldrich Chemical Co., Merck KGaA).

Material synthesis

The exact proportions according to the atomic percentages of Bi, As and Se powder were weighed using an electronic balance. The material was then sealed by an oxygen torch in evacuated (~10^{-5} Torr) quartz ampoule (length ~ 15 cm and internal diameter ~ 1cm). The ampoule containing material was heated to 900 ^{0}C. At that temperature, the ampoule was constantly rocked by rotating the quartz ampoule to obtain homogeneous alloy. After rocking for about 12 hours, the obtained melt was rapidly quenched in ice-cooled water. The quenched sample was then taken out by breaking the quartz ampoule. Thin films of the two different compositions were prepared by thermal evaporation technique (Vacuum coating unit 12A4D**)** using the powder of melt quenched samples as targets. The films were deposited on a glass substrate of size 1 cm × 1 cm and at a base pressure of ~ 1×10^{-5} Torr. Before introducing the substrates inside the vacuum chamber they were cleaned in pure acetone and dried. During the deposition process, the substrates were kept at room temperature and the deposition rate was adjusted at 2 nm/s. The substrates were rotated to obtain a homogenous and smooth film at slow speed during the deposition process. During evaporation process, the thickness of the produced films was measured using quartz crystal thickness monitor. The thickness of the as deposited films was about 800 nm.

Characterization

Surface morphology of the films was characterized by field emission scanning electron microscope (FESEM) of ZEISS SIGMA-40. Elemental composition of the films was determined by Energy Dispersive X-ray analysis (EDX) using the FESEM setup. Grazing incidence X-ray diffraction (GIXRD) for structural study of the prepared films was performed by using Bruker D8 advance X-ray diffractometer with CuK$_\alpha$ radiation (λ= 1.5418 Å). GIXRD measurements in the 2θ range of 10° - 80° of the two films were performed at a grazing angle of 1° with a scan speed of 1^0 /min. Optical transmission of the two films was recorded using Bruker IFS 66v/s UV-Vis-NIR Spectrophotometer in the wavelength range 400-1200 nm.

Results and discussion

Microstructural characterization

The FESEM image of the $As_{40}Se_{60}$ film shows a smooth and homogeneous surface (**Fig. 1**). On the contrary, FESEM image of $Bi_{15}As_{40}Se_{45}$ thin film indicated a rougher surface with granular nature. The average grain size is ~300 nm.

EDX study undertaken at different locations on the surfaces of both the films indicated nearly stoichiometric composition in the film made out of $As_{40}Se_{60}$ target, but a large deviation from the initial composition for the film made out of $Bi_{15}As_{40}Se_{40}$ target. The observed and the expected atomic% of different elements in both the films are shown in **Table. 1**. This table clearly shows that Bi content in the film has reduced drastically to ~4% from the initially taken Bi content of 15% for preparing the target by melt quenching. To compensate for this decrease, both As and Se contents increase. The increase in As content is much more than the increase in Se content. While Se content increases by ~6%, As content increases by ~21%. The drastic reduction of Bi content in the film from that of the initial composition taken for preparing the target is possibly due to evaporation of Bi during melting process inside the ampoule sticking of Bi to the ampoule wall.

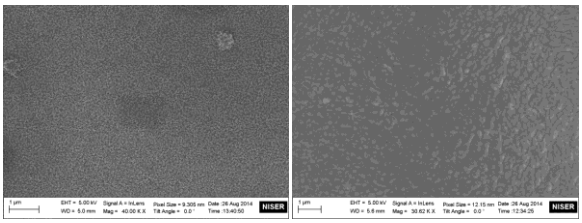

Fig. 1. FE-SEM of $As_{40}Se_{60}$ and $Bi_{15}As_{40}Se_{45}$ thin films respectively.

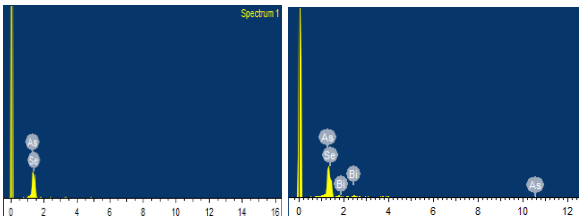

Fig. 2 EDX spectra of $Bi_xAs_{40}Se_{60-x}$ thin films.

Table. 1 The measured elemental composition from EDX for $As_{40}Se_{60}$ and $Bi_{15}As_{40}Se_{45}$ thin films.

	$As_{40}Se_{60}$		$Bi_{15}As_{40}Se_{45}$	
	Atomic% in the films	**Initial Atomic%**	**Atomic% in the films**	**Initial Atomic%**
As	38.8	40	48.5	40
Se	61.2	60	47.6	45
Bi	0	0	3.9	15

Structural Property

Arsenic selenide films of 800 nm thickness with and without bismuth doping were prepared by thermal evaporation using melt quenched targets of $Bi_{15}As_{40}Se_{45}$ and $As_{40}Se_{60}$. To examine the evolution of structure in the bulk and then in the thin film forms, we present the corresponding X-ray diffraction patterns of both the phases in **Fig. 3**. As is seen by many [**20-22**], we also observed amorphous structure of bulk $As_{40}Se_{60}$ (**Fig. 3**). In contrast to $As_{40}Se_{60}$ case, we observed a few XRD peaks for the bulk $Bi_{15}As_{40}Se_{45}$ melt quenched sample (**Fig. 3**).

Comparison of the XRD pattern as given in JCPDS files for different possible elements and compounds, viz. As, Se, Bi, As_2Se_3, Bi_2Se_3 etc. that can form out of As, Se and Bi with our observed XRD pattern indicated formation of Bi_2Se_3 phase. To arrive at this conclusion, we present the observed XRD spectrum of melt quenched $Bi_{15}As_{40}Se_{45}$ sample along with JCPDS data as vertical lines for two prominent possible phases, namely As_2Se_3 and Bi_2Se_3 in **Fig. 3**. This figure clearly shows that though As_2Se_3 is the parent phase in the melt quenched samples, reported XRD pattern of this phase does not match with that of the observed.

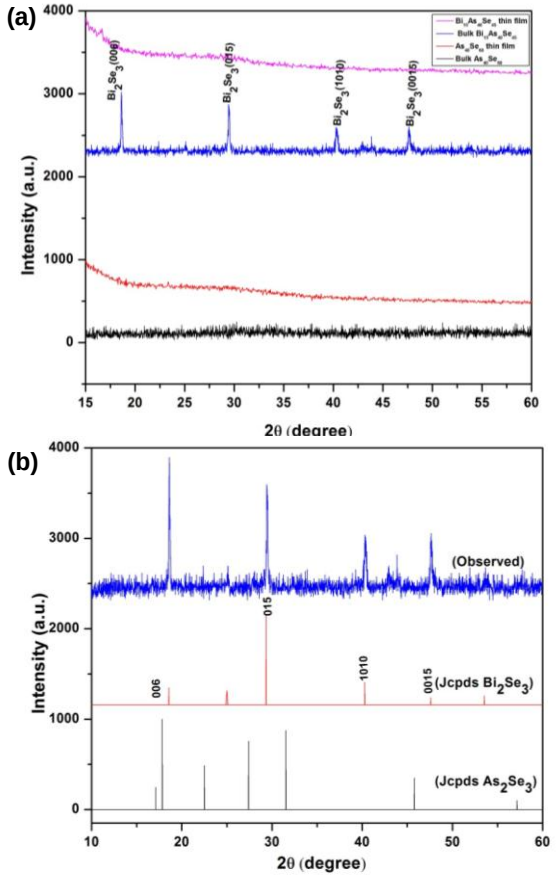

Fig. 3. (a) XRD patterns of both bulk and thin films of $As_{40}Se_{60}$ and $Bi_{15}As_{40}Se_{45}$ thin films (b) XRD of Bi doped bulk As40Se60 along with JCPDS data.

On the contrary, addition of Bi in As_2Se_3 to reach a composition of $Bi_{15}As_{40}Se_{45}$ leads to the formation of Bi_2Se_3 in crystalline form. The diffraction pattern of this phase reported in JCPDS file (33-0214) shows a close matching with the observed XRD pattern in both intensity ratio and position of the lines except for the line occurring at the 2θ of 18.62^0. This line corresponding to the (006) plane of Bi_2Se_3, has a much larger intensity than what is reported in the JCPDS file. The reason for this discrepancy is not clear in the present study. The present study however indicates that in spite of melt quenching, Bi incorporation in As_2Se_3 promotes second phase precipitation in the form of crystalline Bi_2Se_3 phase in the matrix of amorphous As_2Se_3 phase. The size of the Bi_2Se_3 crystallites were estimated from the width of their respective XRD peaks using the Scherrer formula

$$D = \frac{0.9\lambda}{\beta_{2\theta} Cos\theta}$$

where, λ (= 1.54 A^0) is the Cu Kα X-ray wavelength used in the present study, $\beta_{2\theta}$ is the full width at half maximum of the corresponding XRD peak, 2θ is the peak position. We have thus embedded a Bi_2Se_3 nanocrystallites of 46 nm size in an amorphous medium, which can provide avenues for applications in many areas like topological insulators [**23,24**], thermoelectric devices [**25**], optical recording system [**26**], photoelectrochemical devices [**27**] etc.

Optical Property

The transmittance spectra of the deposited films as a function of wavelength are shown in **Fig. 4**. Interference fringes are observed in these spectra beyond 650 nm of wavelength of incident beam. This interference fringes indicate the homogeneity and smoothness of the deposited films. Various optical constants like refractive index, optical absorption coefficient, optical thickness and optical band gap are deduced from the transmittance spectrum [**28, 29**]. The number of interference fringes depends upon the thickness of the films. In our case the thickness of the films is not sufficient to produce more number of interference fringes. Furthermore, the absorption edge of the deposited films shows red shift as the Bi content increases from 0 to 15 at. % as well as transmission spectra peaks shifted towards longer wavelength. This shift is a direct consequence optical band gap of the deposited films. The transmittivity of $Bi_{15}As_{40}Se_{45}$ film decreases as compared to $As_{40}Se_{60}$ in 700-1150 nm range due to defects introduced in the deposited films by the bismuth addition which led to increase in light absorption [**30**].

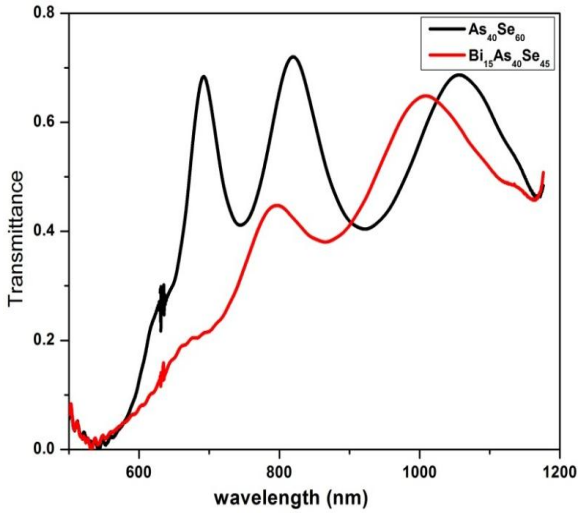

Fig. 4. Transmission spectra of $As_{40}Se_{60}$ and $Bi_{15}As_{40}Se_{45}$ thin film.

Absorption coefficient and optical band gap

Whenever any electromagnetic wave propagates inside the medium, its loss by absorption or scattering process is represented by absorption coefficient. The absorption coefficient, α of $Bi_xAs_{40}Se_{60-x}$ (x = 0, and15 at. %) amorphous thin films are calculated from the experimental data of transmittance in strong absorption region using the relation

$$\alpha = \frac{1}{d} ln \frac{1}{T}$$

where T is the transmittance and d is the thickness of the deposited films.

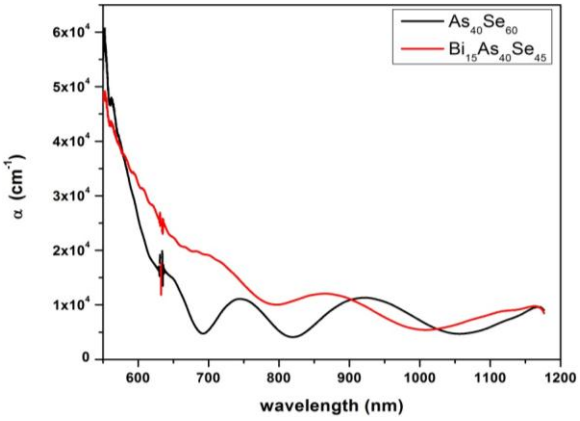

Fig. 5. Variation of α with λ in $As_{40}Se_{60}$ and $Bi_{15}As_{40}Se_{45}$ thin films.

At a particular wavelength there is an increase in the value of absorption coefficient (α) for $Bi_xAs_{40}Se_{60-x}$ thin films. The reduction of α with wavelength shows that the material is getting transparent at higher wavelength, which makes it a useful optical material in higher wavelength range. The absorption coefficient is found to be increased for the $Bi_{15}As_{40}Se_{45}$ than the $As_{40}Se_{60}$ film. Due to the large absorption coefficient, these materials may be suitable for optical memory devices as well as in solar cells.

The relation between absorption coefficient (α) and the incident photon energy (hν) be written as [**31**].

$$\alpha h\nu = B(h\nu - E_g)^n \quad (1)$$

where, B is a constant called Tauc parameter and it is a measurement of disorder and n is an index which depends on the nature of electronic transition responsible for the optical absorption. Values of n for allowed direct and non-direct transitions are 1/2 and 2, respectively [**32**].

The corresponding E_g values are obtained by extrapolating the straight line portion of the graph on hν axis as shown in **Fig. 6**. The indirect optical band gap values calculated from $(\alpha h\nu)^{1/2}$ vs hν are listed in **Table. 2**. It is shown from Table. 2 that the values of optical band gap (Eg) decreases from 1.74 eV (As40Se60) to 1.28 eV (Bi15As40Se45) with increase in Bi content at the expense of Se content. Decrease band gap with increasing Bi concentration indicates formation of defect states leading to the presence of localized states in the band gap.

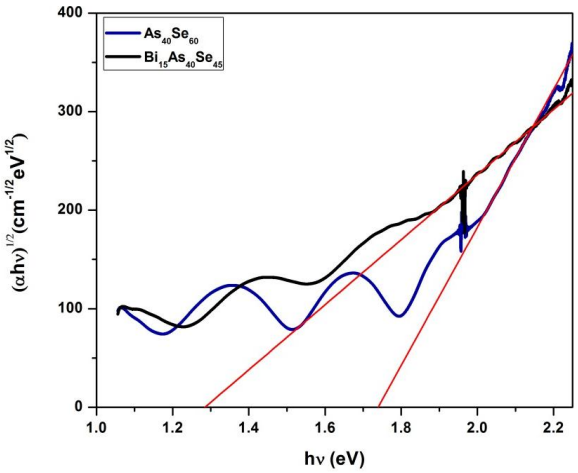

Fig. 6. $(\alpha h\nu)^{1/2}$ vs (hν) plots for $As_{40}Se_{60}$ and $Bi_{15}As_{40}Se_{45}$ thin films

Table. 2 Optical constants of $As_{40}Se_{60}$ and $Bi_{15}As_{40}Se_{45}$ thin films

Sample	Optical band gap E_g (eV)	Tauc parameter $B^{1/2}$ ($cm^{-1/2}eV^{-1/2}$)
$As_{40}Se_{60}$	1.74	700
$Bi_{15}As_{40}Se_{45}$	1.28	330

Similar trend of decreasing optical band gap with increasing Bi concentration have been observed by other authors in $Ge_{20}Bi_xSe_{80-x}$ and $Se_{80-x}Te_{20}Bi_x$ thin films [**33, 34**]. The decrease in optical band gap with increase of the Bi content can be explained on the basis of Mott and Davis Model [**35**]. According to this model, chalcogenide thin films contain a high concentration of defect states and these defects are responsible for the presence of localized states in the band gap. The model proposed that the width of the localized states near the mobility edges depends on the degree of disorder and defects present in the amorphous structure. In particular, it is known that unsaturated bonds together with some saturated bonds are produced as the result of an insufficient number of atoms deposited in the amorphous film. The decrease in optical band gap along with the increase in the density of defect states may also be correlated with the electronegativity of the elements present in the sample. Bi has lower electronegativity than Se. The valence band of chalcogenides contain the lone pair P-orbital and the addition of electropositive element (Bi) to electronegative element (Se) may raise the energy of lone pair states, which is further responsible for the broadening of valence band inside the forbidden gap which leads to decrease of band gap [**34**].

The slope of the fitting in equation 1 gives the value of $B^{1/2}$. The constant B includes information on the convolution of the valence band and conduction band states and on the matrix element of optical transitions, which reflects not only the k selection rule but also the disorder induced spatial correlation of optical transitions between the valence band and conduction band [**36**]. Moreover, B is highly dependent on the character of the bonding [**37**]. The values of $B^{1/2}$ for $As_{40}Se_{60}$ and $Bi_{15}As_{40}Se_{45}$ films are found to be 700 and 333 $cm^{-1/2}eV^{-1/2}$ respectively. This decrease in tauc parameter indicates the increase in disorderness due to which the band tail extends into the gap region which results in the decrease of optical band gap. This indicates the presence of more no of homopolar bonds in the $Bi_{15}As_{40}Se_{45}$ film.

Conclusion

The present study has shown that Bi incorporation in $As_{40}Se_{60}$ with composition $Bi_{15}As_{40}Se_{45}$ leads to nucleation of Bi_2Se_3 nanocrystallites in a glassy matrix prepared through melt quenching technique. The films made out of this target is amorphous and does not show any crystallinity. The actual concentration of Bi in the film is much less than the initial concentration taken for making the target. Even with much less Bi content (~4%), optical band gap of the film shows a large decrease from that of the film without Bi content. The transmittance also decreases with addition of Bi into $As_{40}Se_{60}$. Decrease of band gap with increasing Bi concentration indicates formation of defect states leading to the presence of localized states in the band gap. The FESEM images show smooth and homogeneous surface for $As_{40}Se_{60}$ thin film.

Acknowledgements

One of the authors M. Behera would like to thank IUAC, New Delhi for financial support through junior research fellowship and also the authors thank DST for DST-INSPIRE Faculty Research Grant.

Author's contributions

Conceived the plan: R.Naik; Performed the expeirments: M.Behera; Data analysis: M.Behera , R.Naik. R. Panda,and N.C. Mishra; Wrote the paper: M. Behera. Authors have no competing financial interests.

References

1. Savage, J. A.; Infrared Optical Materials and Their Antireflection Coatings; London: Hilger, **1985.**
2. Shiryaev V. S.; Boussard-Pl´edel, C.; Houizot, P.; Jouan, T.; Adam, J. L.; Lucas, J.; *Mater. Sci. Eng. B*, **2006,** *127*, 138.
3. King, W. A.; Clare, A. G.; Lacourse, W. C.; *J. Non-Cryst. Solids*, **1995,** *181*, 231.
4. Tauc, J.; Amorphous and Liquid Semiconductors Chap. 4, New York: Plenum **1974.**
5. Minkov, D.; Vateva, E.; Skordeva, E.; Arsova, D.; Nikiforova, M.; *J. Non-Cryst. Solids*, **1987,** *90*, 481.
6. Kosek, F.; Cimpl, Z.; Tulka, J.; Chlebny, J.; *J. Non-Cryst. Solids*, **1987**, *90*, 401.
7. Borisova, Z. U.; Glassy Semiconductors Plenum Press, New York, **1981**.
8. Ohta, T.; *J. Optoelectron. Adv. Mater*, **2001**, *3*, 609.
9. Lankhorst, M.H.R; Ketelaars, B. W. S. M. M.; Wolters, R. A. M.; *Nat. Mater*, **2005**, *4*, 347.
10. Churbanov, M.F.; Snopatin, G.E. ; Shiryaev, V.S. ; Plotnichenko, V.G. ; Dianov, E.M.; *J. of Non Cryst. Solids*, **2011**, *357*, 2352.
11. Pandey, V.; Tripathi, S. K.; Kumar, A. J.; *Ovonic Res.*, **2007**, *3*, 229.
12. Golovchak, R.; Shpotyuk, Ya.; Nazabal, V.; Boussard-Pledel, C.; Bureau, B.; Cebulski, J.; Jain, H.; J.; Che. Phys., **2015**, *142*, 184501
13. Sharma, P.; Sharma, V.; Barman, P.B.; Katyal, S.C.; *Optoelectron. Adv. Mater., Rapid Commun*., **2012**, *6*, 804.
14. Kumar, S.; Kashyap, S. C.; Chopra, K. L.; *J. Appl Phys.*, **1992**, *72*, 2066.
15. Golovchak, R.; Shpotyuk, O.; Kovalskiy, A.; Miller, A. C.; Čech, J.; Jain, H.; *Phys. Rev. B*, **2008**, *77*, 172201.
16. El-Samanoudy, M. M.; *Thin Solid Films*, **2003,** *423***,** 201.
17. Irfan, B.; Sahoo, S.; Gaur, A. P. S.; Ahmadi, M.; Guinel, J.-F., M.; Katiyar, R. S.; Chatterjee, R.; *J. Appl. Phys.*, **2014**, *115*, 173506.
18. Barzola-Quiquia, J.; Lehmann,T.; Stiller, M.; Spemann, D.; Esquinazi, P.; Häussler, P.; *J.Appl.Phys*, **2015**, *117*, 075301.
19. Suthan Kissinger, N.J.**;** Preparation And Properties Of Chalcogenide Materials For Solar Cells; Lambert: Germany, **2015.**
20. Singh, M.; Bhatia, K.L.; Kishore, N.; Kundu, R.S.; Kanjilal, D.; *Nucl. Instru. Method. Phys. Res. B*, **1998**, *140*, 349.
21. Sati, D.C.; Kumar, R.; Mehra,R.M.; *Turkish J. Phys.*, **2006,** *30*, 519.
22. Chauhan, R.; Tripathi, A.; Srivastava, K. K.; *Materials International*, **2014,** *24*, 239.
23. Zhao, Z.; Wang, S.; Oganov, A. R.; Chen, P.; Liu, Z.; Mao, W. L.; *Phys. Rev. B*, **2014**, *89*, 180102.
24. Zhang, H.; Liu, C. X.; Qi, X. L.; Dai, X.; Fang, Z.; Zhang, S. C.; *Nat. Phys.*, **2009,** *5*, 438.
25. Bayaz, A.A.; Giani, A.; Foucaran, A.; Pascal-Delannoy, F.; Boyer, A.; *Thin Solid Films*, **2003**, *441*, 1.
26. Watanabe, K.; Sato, N.; Miyaoko, S.; *J Appl Phys*, **1983**, *54*, 1256.
27. Waters, J.; Crouch, D.; Raftery, J.; O'Brien, P.; *Chem Mater*., **2004**, *16*, 3289.
28. Naik, R.; *Adv. Mater. Lett.*, **2015**, *6*, 531.
29. Swanepoel, R.; *J. Phys. E: Sci. Instrum***., 1983,** *16*, 1214.
30. Mulama, A.A.; Mwabora, J.M.; Oduor, A. O.; Muiva, C. M.; Muthoka, B.; Amukayia, B.N.; Mbete, D .A.; *New J. Glass Ceram.*, **2015**, *5*, 16.
31. Tauc, J.; Amorphous and liquid semiconductor, New York, Plennum Press **1974**, 179.
32. Naik, R.; Jena, S.; Ganesan, R.; Sahoo, N. K.; *Phys. Status Solidi B*, **2014**, *251*, 661.
33. Korashya, A. E.; Kabanya, N. E.; Zahed, H. E.; *Physica B*, **2005**, *365*, 55.
34. Sharma, K.; Lal, M.; Goyal, N.; *J. Optoelectron. Biomed. Mater.*, **2014**, *6*, 27.
35. Mott, N.F.; Davis, E.A.; Electronic process in Non-crystalline materials, Claredon: Oxford, **1979,** pp-382/428.
36. Zanatta, A.R.; Chambouleyron, I.; *Phys. Rev. B*, **1996**, *53***,** 3833.
37. Dow, J.D.; Redfield, D.; *Phys. Rev. B*, **1970**, *1*, 3358.

